Pulse Electrodeposition of CuO/Cu_2O on 3D-Printed Nickel-Containing Carbon Structures for Visible-Light Photocatalytic Degradation of Methylene Blue

B.Tech Project Report

Submitted by

Nikita Sewda (B22ME042) , Ojasvi Pandey (B22ME043)

Under the Supervision of

Prof. Ankur Gupta

Prof. Chandan Pandey

Department of Mechanical Engineering

Indian Institute of Technology Jodhpur

November, 2025

Acknowledgements

We would like to express our sincere gratitude to Prof. Ankur Gupta and Prof. Chandan Pandey, Department of Mechanical Engineering, IIT Jodhpur, for their invaluable guidance and continuous support throughout this project. Their expertise in materials science and electrochemistry has been instrumental in shaping this research.

We are thankful to Divyansh Mittal and Achutya Mishra and the laboratory staff and technical personnel at IIT Jodhpur for providing access to characterization facilities, including SEM, EDS, XRD, and Raman spectroscopy. We also acknowledge our peers and colleagues for their constructive feedback and discussions that enriched our understanding of photocatalytic systems.

Finally, we express our gratitude to our families for their constant encouragement and support during the course of this project.

Abstract

Water contamination by organic dyes, particularly methylene blue (MB) from textile industries, poses a severe threat to public health and ecosystems in India. With 820 million people facing extreme water stress and 200,000 annual deaths attributed to poor water quality, there is an urgent need for efficient, sustainable water treatment technologies. This project investigates the photocatalytic degradation of methylene blue using pulse electrodeposition of copper oxide (Cu_2O/CuO) on 3D-printed nickel-containing pyrolytic carbon (PyC) microlattice structures.

The microlattice design provides high surface area, deep light penetration, and abundant active sites for pollutant degradation. Samples were prepared with varying nickel content (0.5%, 1%, 5%, and 10%) in the carbon substrate, followed by pulse electrodeposition of Cu_2O and silver (Ag) nanowire decoration to enhance photocatalytic performance. Comprehensive characterization using SEM, EDS, XRD, and Raman spectroscopy revealed that 5% Ni content yields optimal Cu_2O deposition with superior crystallinity and uniform surface coverage.

The photocatalytic tests demonstrated that the 5% Ni sample with Ag decoration achieved maximum methylene blue degradation under visible light irradiation. The study elucidates the critical role of nickel in facilitating electron transfer, promoting nucleation sites, and stabilizing local pH during electrodeposition. However, excessive Ni content (10%) leads to reduced Cu_2O formation due to overly conductive surfaces favoring metallic copper formation and competing hydrogen evolution reactions.

This work establishes an optimized fabrication strategy for advanced photocatalytic materials and demonstrates the potential of 3D microlattice structures for sustainable water purification applications.

Keywords: Photocatalysis, Copper oxide, Pyrolytic carbon, Electrodeposition, Methylene blue degradation, Water treatment

Contents

1

Introduction

1.1 Objective

The primary objective of this project is to compare the photocatalytic performance of Cu_2O@PyC and (Ag/Cu_2O)@PyC microlattice structures for efficient degradation of methylene blue in water under visible light irradiation.

Specific objectives include:

- Fabricate 3D pyrolytic carbon (PyC) microlattice structures with varying nickel content (0.5%, 1%, 5%, and 10%) using DLP 3D printing followed by pyrolysis.
- Deposit Cu_2O/CuO coatings on the carbon substrates using the pulse electrodeposition technique.
- Enhance photocatalytic activity through surface decoration with silver nanowires.
- Characterize the morphological, structural, and optical properties of the synthesized photocatalysts.
- Evaluate the photocatalytic degradation efficiency of methylene blue under visible-light exposure.
- Compare the photocatalytic performance of Cu_2O@PyC and (Ag/Cu_2O)@PyC microlattice structures for efficient degradation of methylene blue under visible light irradiation.
- Determine the optimal nickel content for maximum Cu_2O deposition and photocatalytic performance.
- Elucidate the mechanisms linking nickel content to Cu_2O formation and overall photocatalytic behavior.

1.2 Background

1.2.1 Background and Motivation

Water scarcity and contamination represent one of the most pressing challenges facing India today. Current statistics paint a concerning picture: approximately 820 million people in India experience high to extreme water stress, and tragically, 200,000 Indians die annually due to inadequate water quality. Projections suggest that by 2030, water scarcity could displace 700 million people globally, with India being among the most severely affected regions.

The textile industry, one of India's largest manufacturing sectors, is a major contributor to water pollution. This industry consumes vast quantities of water and discharges large volumes of wastewater containing various organic dyes, with methylene blue (MB) being one of the most prevalent and hazardous pollutants. Methylene blue is a cationic thiazine dye extensively used in textile dyeing, paper printing, and as a biological stain.

Health Impacts of Methylene Blue Contamination:
Exposure to methylene blue in contaminated water sources leads to severe health complications:

- **Tissue necrosis:** Death of body tissue upon contact or ingestion.
- **Cyanosis:** Oxygen deprivation causing characteristic blue discoloration of the skin.
- **Respiratory distress:** Difficulty breathing and compromised lung function.
- **Cardiovascular complications:** Heart-related issues and circulatory system damage.
- **Gastrointestinal effects:** Severe vomiting and disruption of digestive processes.
- **Jaundice:** Liver dysfunction leading to yellowing of the skin and eyes.
- **Neurological damage:** Long-term impairment of nervous system function.
- **Carcinogenic and mutagenic properties:** Potential to induce cancer and genetic mutations.
- **High toxicity:** Lethal effects even at relatively low concentrations.

The persistence of methylene blue in aquatic ecosystems further compounds the problem, as it inhibits photosynthesis in aquatic plants, disrupts oxygen levels, and bioaccumulates in the food chain. Conventional water treatment methods such as adsorption, coagulation, and biological treatment often prove inefficient for complete removal of these stable dye molecules. Photocatalysis has emerged as a promising advanced oxidation process (AOP) for degrading organic pollutants. This technology harnesses light energy to generate reactive oxygen species

(ROS) that mineralize organic contaminants into harmless products like CO_2 and H_2O. However, the efficiency of photocatalytic systems depends critically on the catalyst material, its surface area, light absorption characteristics, and charge carrier dynamics.

1.2.2 Advantages of Pyrolytic Carbon Microlattice Structure

The selection of a 3D pyrolytic carbon microlattice as the substrate for photocatalyst deposition offers several distinct advantages over conventional planar or powder-based photocatalytic systems:

1. Enhanced Light Penetration: The open microlattice architecture allows UV/visible light to penetrate deep into the (Ag/Cu_2O)@PyC structure rather than being limited to surface interactions. This three-dimensional exposure maximizes photon absorption throughout the material volume, leading to uniform generation of reactive oxygen species (ROS) across the entire catalyst structure. In contrast, dense or planar catalysts suffer from light scattering and absorption limitations that reduce overall efficiency.

2. High Surface Area: The interconnected strut network of the microlattice provides an exceptionally high surface-area-to-volume ratio.
This geometric advantage enables:

- Greater catalyst loading capacity per unit volume.
- More active sites available for pollutant adsorption and degradation.
- Increased contact area between the catalyst and contaminated water.
- Enhanced mass transfer of reactants and products.

3. Improved Mass Transport: The porous geometry facilitates efficient fluid flow through the structure, ensuring:
Continuous supply of fresh contaminated water to active sites Rapid removal of degradation products preventing surface blocking Minimized diffusion limitations commonly encountered in dense catalyst beds Better mixing and distribution of reactive species.

4. Structural Stability: Pyrolytic carbon derived from polymer precursors exhibits:
Excellent mechanical strength to withstand handling and flow conditions Chemical inertness providing stability across wide pH ranges Thermal stability allowing for high-temperature processing steps Long-term durability for repeated photocatalytic cycles.

5. Electrical Conductivity: The conductive carbon framework serves multiple functions:
Acts as an electron sink, accepting photogenerated electrons from Cu_2O Reduces electron-

hole recombination, a major efficiency limitation in semiconductors Facilitates rapid charge transport away from generation sites Enables electrochemical deposition of active materials.

6. Nickel Enhancement Effect: The incorporation of nickel particles within the carbon matrix further amplifies these benefits by:

Improving electrical conductivity beyond pure carbon.

Providing catalytic sites for controlled electrodeposition.

Creating high-energy nucleation centers for uniform Cu_2O growth

Modulating local electrochemical conditions during deposition.

This combination of structural, electrical, and chemical properties makes the nickel-containing pyrolytic carbon microlattice an ideal platform for advanced photocatalytic applications, addressing key limitations of traditional photocatalyst configurations.

2

Work Done

2.1 Methodology

The experimental approach consisted of four major phases:

- Design and fabrication of 3D microlattice structures.
- Conversion of the printed structures into pyrolytic carbon through controlled pyrolysis.
- Pulse electrodeposition of copper oxide onto the carbon framework.
- Silver nanowire decoration to enhance photocatalytic performance.

The methodology integrates additive manufacturing with electrochemical processing techniques, leveraging the strengths of each approach. Digital Light Processing (DLP) 3D printing enables precise control over complex geometries that would be impossible to achieve through conventional manufacturing. Subsequent pyrolysis converts the polymer matrix into conductive carbon while preserving the designed microarchitecture. Electrodeposition allows conformal coating of CuO on the intricate surfaces, and finally, drop-casting introduces silver enhancement.

2.1.1 Sample Preparation and Fabrication

- **Step 1: CAD Design** The microlattice was created using CAD software to generate a periodic 3D architecture of interconnected struts. Design parameters were optimized to ensure:
  - Sufficient strut thickness for mechanical integrity
  - Adequate porosity for light penetration and fluid flow
  - Large surface area for catalyst loading

  - Printability within DLP printer capabilities

  The final model was exported as an STL file for printing.

- **Step 2: Slicing and Print Preparation** The STL was imported into slicing software and divided into thin layers. Key slicing parameters included:
  - Layer thickness (resolution vs. print time)
  - Exposure time per layer (calibrated for the resin)
  - Support structures (added for overhangs)

- **Step 3: DLP 3D Printing** The structures were printed using DLP technology with PEGDA resin containing dispersed Ni particles (0.5%, 1%, 5%, 10%). The process involved:
  - UV projection patterning each layer
  - Photopolymerization of exposed regions
  - Incremental lifting of the build platform
  - Embedding of Ni particles in the polymer matrix

  Advantages of DLP include high resolution, fast curing, uniform Ni distribution, and ability to fabricate complex geometries.

- **Step 4: Post-Processing** After printing, the parts underwent:
  - Washing in isopropanol to remove uncured resin
  - Drying at room temperature
  - UV post-curing for complete polymerization

- **Step 5: Pyrolysis** Printed polymer–Ni composites were converted into pyrolytic carbon under controlled conditions:
  - Temperature: 900°C
  - Atmosphere: Argon or nitrogen
  - Heating rate: 5–10°C/min
  - Holding time: 1–2 hours
  - Cooling: Slow cooling under inert atmosphere

  Pyrolysis mechanism:
  - 200–400°C: Depolymerization and volatilization
  - 400–700°C: Chain scission and aromatic formation
  - 700–900°C: Graphitization into an sp^2 carbon network

Final result: porous pyrolytic carbon preserving the original microlattice geometry.

The embedded nickel particles remain intact during pyrolysis, becoming dispersed within the carbon matrix. The resulting 3D-PEGDA/Ni@PyC structure exhibits:

Electrically conductive carbon framework Preserved microlattice architecture with some dimensional shrinkage (30-40%) Embedded nickel particles enhancing conductivity and catalytic properties Increased surface roughness beneficial for subsequent deposition

2.1.2 Electrochemical Deposition Process

Copper oxide was deposited onto the pyrolytic carbon substrates using pulse electrodeposition, an electrochemical technique offering superior control over deposit morphology compared to continuous deposition.
Electrolyte Composition: The electroplating bath was prepared with the following components:

- Copper sulfate pentahydrate ($CuSO_4 \cdot 5H_2O$), 0.75% — Source of Cu^{2+} ions.
- Sodium hydroxide (NaOH), 1.6% — Provides an alkaline medium favoring Cu_2O formation.
- Lactic acid, 3.9% — Acts as a complexing agent that controls Cu^{2+} reduction kinetics.

The alkaline pH (achieved through NaOH) is critical because it stabilizes the Cu oxidation state necessary for Cu_2O formation. In neutral or acidic conditions, metallic copper (Cu) would preferentially deposit. Lactic acid acts as a chelating agent, forming copper-lactate complexes that moderate the reduction rate, leading to more controlled and uniform CuO nucleation.

Pulse Electrodeposition Parameters:

- Frequency: 50 Hz — Number of pulses per second.
- Voltage: 5 V — Applied potential difference.
- Duty Cycle: 40% — Ratio of ON-time to total cycle time.

Pulse Deposition Advantages:
Pulsed current offers significant benefits over direct current (DC) deposition:

- **Improved morphology:** During the OFF-time, the concentration gradient near the electrode relaxes, allowing fresh Cu^{2+} ions to diffuse to the surface, leading to more uniform coverage.

- **Better nucleation control:** Pulse parameters can be tuned to favor nucleation over growth, producing finer grain structures with more grain boundaries (active sites).
- **Reduced concentration polarization:** OFF periods allow the diffusion layer to recover, minimizing mass transport limitations.
- **Enhanced adhesion:** The intermittent nature of pulsing promotes stronger mechanical bonding between the deposited layer and the substrate.

Electrochemical Reactions: At the cathode (PyC substrate):

$$Cu^2 + e \rightarrow Cu^+$$
$$2Cu^+ + H_2O + 2e^- \rightarrow Cu_2O + 2H^+$$

The alkaline conditions and controlled reduction kinetics favor the two-step process forming cuprous oxide (Cu_2O) rather than direct reduction to metallic copper. Some surface oxidation may also produce cupric oxide (CuO), particularly upon exposure to air after deposition.

Experimental Setup:

- Working electrode: 3D-PEGDA/Ni@PyC microlattice.
- Counter electrode: Platinum or graphite.
- Reference electrode: Saturated calomel electrode (SCE) or Ag/AgCl.
- Configuration: Three-electrode system operated under potentiostat control.

The samples were immersed in the electrolyte and the pulse voltage applied for a predetermined time (typically 10-30 minutes) until desired Cu_2O loading was achieved.

2.1.3 Silver Nanowire Decoration

After Cu_2O deposition, selected samples were further enhanced with silver nanowires through drop-casting.

Process:
Silver nanowire suspension prepared in ethanol or water Controlled volume (e.g., 50-100 L) dropped onto Cu_2O-coated samples Solvent evaporation at room temperature or mild heating (40-60°C) Ag nanowires deposited preferentially at strut intersections and along Cu_2O surface

Role of Silver:

- **Plasmonic enhancement:** Ag nanostructures exhibit localized surface plasmon resonance (LSPR) in the visible range, increasing local electromagnetic field intensity and light absorption.
- **Electron sink:** Ag can accept photogenerated electrons due to favorable energy band alignment, thereby reducing electron–hole recombination.
- **Co-catalyst:** Ag may catalyze specific reactive oxygen species (ROS) generation pathways, enhancing photocatalytic activity.
- **Hot electron injection:** Under certain conditions, plasmonically excited Ag can inject energetic electrons into the Cu_2O conduction band.

The final samples were designated as:

3D-PEGDA/x%Ni_Cu_2O
(3D-PEGDA/x%Ni_Cu_2O_Ag (where x = 0.5, 1, 5, 10)

2.1.4 Characterization Techniques

Comprehensive characterization was performed to understand the structural, morphological, compositional, and optical properties of the synthesized photocatalysts.

- **Scanning Electron Microscopy (SEM)** SEM was used to observe surface morphology and microstructural features of the microlattice across multiple scales.
  - Principle: A focused electron beam scans the surface; emitted secondary electrons, backscattered electrons, and X-rays generate high-resolution images.
  - Analysis performed:
    * Surface topography of carbon struts
    * Cu_2O deposit morphology and distribution
    * Coverage uniformity across the microlattice
    * Particle size and shape of deposits
    * Multiple magnifications (100× to 10000×) to capture macro– to nanoscale features
- **Field Emission Scanning Electron Microscopy (FESEM)** FESEM provides higher-resolution imaging due to its field emission source.
  - Advantages:
    * Superior resolution for nanoscale features
    * Clearer visualization of Cu_2O crystallites

    - Better depth of field for 3D structures
    - Enhanced contrast for Ag nanowire identification
  - FESEM at 5000× and 10000× helped visualize Ag nanowires decorating Cu_2O, especially at strut junctions.

- **Energy Dispersive X-ray Spectroscopy (EDS)** EDS provided elemental analysis and spatial distribution mapping.
  - Principle: Electron beam excites atoms; emitted characteristic X-rays reveal elemental identity.
  - Information obtained:
    - Confirmation of Cu, O, Ag, C, and Ni
    - Semi-quantitative elemental composition
    - Elemental mapping across the microlattice
    - Verification of deposition success
  - EDS mapping showed 5% Ni sample had the highest and most uniform Cu deposition.

- **X-ray Diffraction (XRD)** XRD identified crystal phases and confirmed structural information.
  - Principle: X-rays diffract according to Bragg's law ($n\lambda = 2d\sin\theta$), producing phase-specific patterns.
  - Analysis included:
    - Phase identification
    - Confirmation of Cu_2O (cuprite) formation
    - Detection of Ag in decorated samples
    - Crystallinity assessment from peak sharpness
    - Crystallite size estimation (Scherrer equation)
  - Key observations:
    - Cu_2O peaks: 30°, 36°, 42°, 62°, 73°
    - Ag peaks: 38°, 44°, 64°

- **Raman Spectroscopy** Raman analysis provided molecular vibrational information.
  - Principle: Inelastic scattering causes energy shifts corresponding to vibrational modes.
  - Cu_2O identification:
    - Cu_2O exhibits a characteristic vibrational mode at $150\ \text{cm}^{-1}$
    - This confirms Cu_2O formation and crystalline quality
  - Raman intensity trend followed Ni-dependent Cu_2O formation:

    * 0.5% → 1% → highest at 5% → drop at 10% Ni

- **UV–Visible Spectroscopy** UV–Vis spectroscopy assessed optical properties and photocatalytic degradation.
  - Applications:
    * Optical absorption study
    * Band gap estimation (Tauc plot)
    * Monitoring methylene blue degradation kinetics
    * Quantifying photocatalytic efficiency
  - Methylene Blue Monitoring:
    * MB has a strong absorption peak at 664 nm
    * Degradation monitored by decrease in absorbance over time
    * Formula:

$$\text{Degradation } (\%) = \frac{(C_0 - C_t)}{C_0} \times 100$$

3

Results and Discussion

3.1 Morphological Analysis (SEM/FESEM)

3.1.1 SEM Imaging of Cu_2O-Coated Samples

Scanning electron microscopy revealed distinct morphological differences across samples with varying nickel content. Images were captured at multiple magnifications (100×, 200×, 500×, 1000×, 5000×, 10000×) to assess both macroscopic coverage and microscopic crystal structure. General Observations: At lower magnifications (100×-500×), all samples exhibited the preserved microlattice architecture with interconnected struts forming periodic three-dimensional networks. The pyrolysis process caused some dimensional shrinkage but maintained structural integrity without cracking or collapse. At higher magnifications (5000×-10000×), the CuO deposits appeared as rough, granular coatings on the PyC struts. The morphology consisted of small clustered deposits indicating successful nucleation and growth on the carbon surface. The grain size, coverage density, and uniformity varied significantly with Ni content:

- 0.5% Ni: Sparse Cu_2O coverage with isolated particle clusters; large bare carbon regions visible; inconsistent deposit distribution.
- 1% Ni: Improved coverage compared to 0.5%; more continuous film formation, but still significant gaps in the coating.
- 5% Ni: Dense, uniform Cu_2O coating across all strut surfaces; fine-grained structure with high nucleation density; minimal exposed carbon substrate; most homogeneous distribution.
- 10% Ni: Reduced coverage compared to 5%; patchy, non-uniform deposits; larger grain sizes indicating reduced nucleation and coarsened growth.

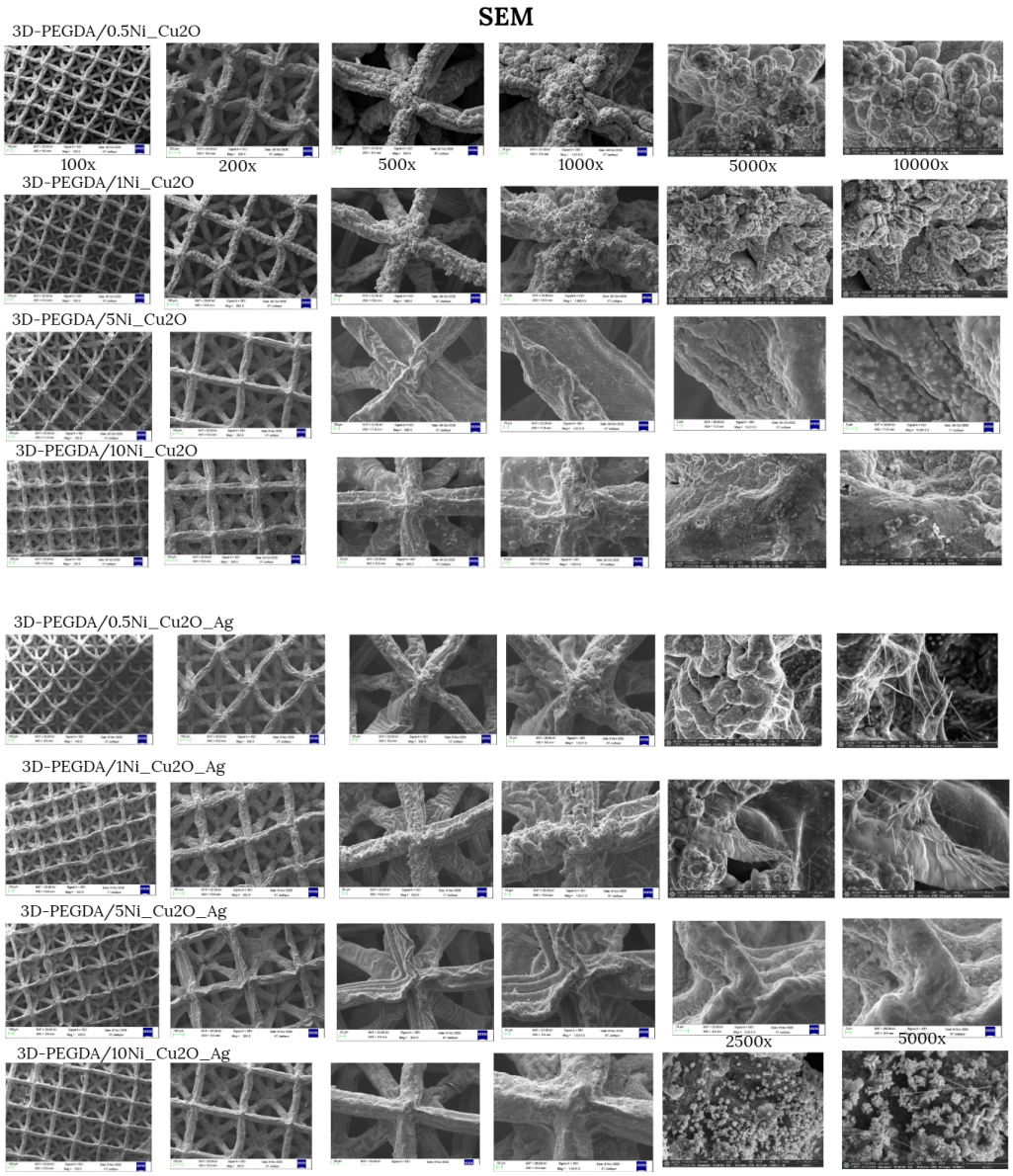

3.1.2 FESEM Imaging of Ag-Decorated Samples

Higher resolution FESEM imaging (5000×-10000×) of Ag-decorated samples revealed additional nanoscale features:

- Ag nanowire identification: Thin, elongated wire-like structures observed on top of the Cu_2O layer.
- Preferential decoration: Ag features are concentrated around strut intersections and joints where the drop-cast solution accumulated.
- Morphology: Presence of flake-like and wire-like geometries with high aspect ratios characteristic of Ag nanowires.
- Cu_2O/Ag interface: Clear distinction between the underlying granular Cu_2O surface and the overlying Ag nanostructures.

The FESEM images confirmed successful multi-component catalyst fabrication with hierarchical structure: carbon substrate → Cu_2O layer → Ag nanowire decoration.

3.2 Elemental Composition (EDS)

Energy dispersive X-ray spectroscopy provided quantitative elemental analysis and spatial distribution mapping.
Elemental Identification:
EDS spectra confirmed the presence of expected elements:

- Carbon (C): Major constituent originating from the pyrolytic carbon substrate.
- Oxygen (O): Present due to Cu_2O/CuO deposits.
- Copper (Cu): Derived from the electrodeposited oxide layer.
- Nickel (Ni): Embedded within the carbon matrix from the 3D printing process.
- Silver (Ag): Detected only in Ag-decorated samples.

Quantitative Analysis:
While EDS provides semi-quantitative composition, the relative peak intensities offered valuable comparative information across samples. Cu signal intensity served as a proxy for deposition amount:

EDS

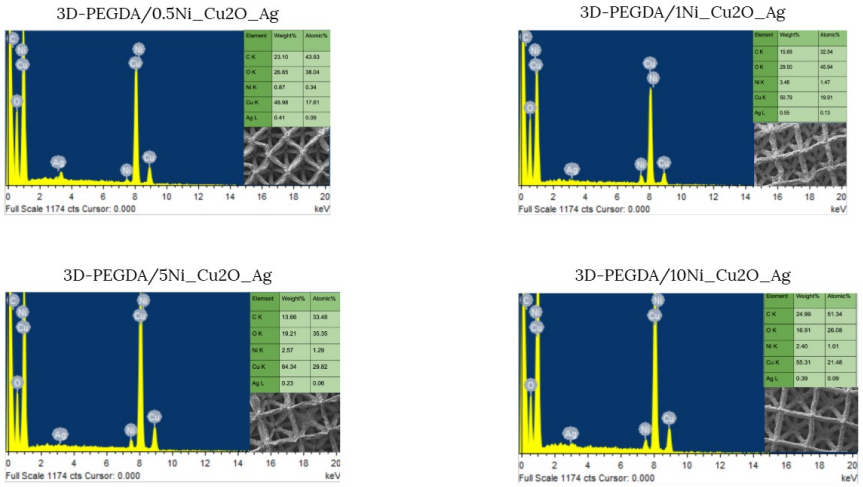

- 0.5% Ni: Weak Cu signal; low atomic percentage.
- 1% Ni: Moderate Cu signal; improved compared to 0.5%.

- 5% Ni: Strongest Cu signal; highest atomic percentage.
- 10% Ni: Reduced Cu signal compared to 5%.

Elemental Mapping: Color-coded elemental maps visually demonstrated spatial distribution:
Cu_2O Samples: The Cu mapping (typically displayed in red or green) showed:

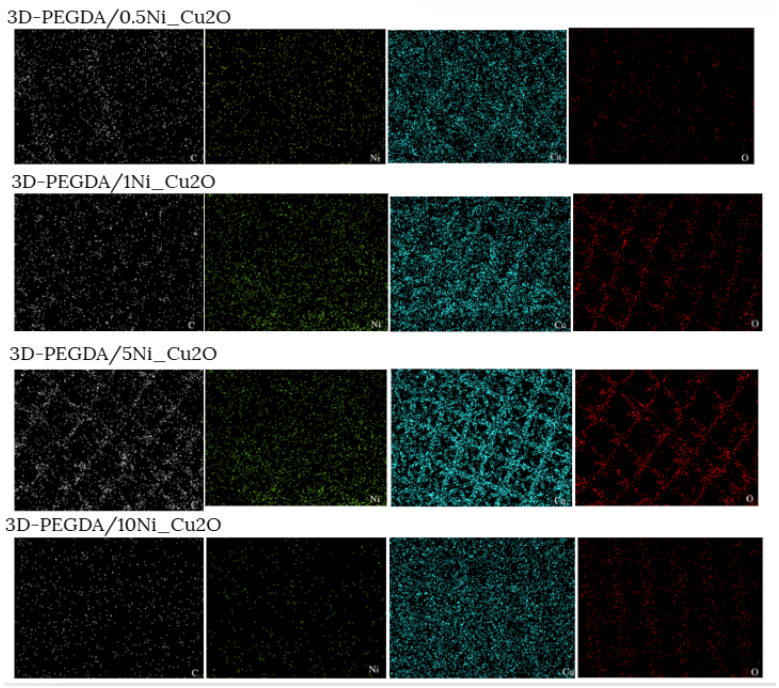

Progressive increase in Cu distribution density from 0.5% → 1% → 5% Ni
5% Ni sample exhibited the densest, most uniformly spread Cu signal across the analyzed region.
10% Ni showed scattered, less uniform Cu distribution.

Ag-Decorated Samples:
Additional Ag mapping confirmed.

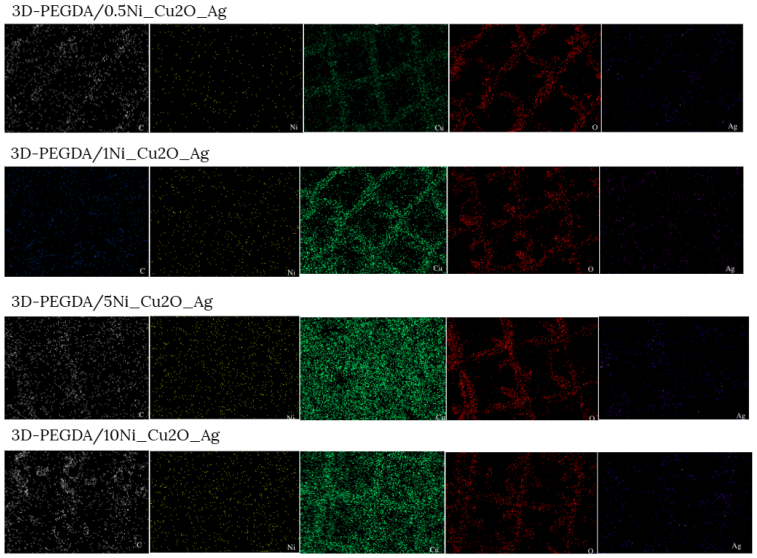

Successful Ag nanowire deposition on all decorated samples. Ag signal localized primarily on surface and strut junctions. Co-localization of Cu and Ag signals indicating intimate contact between layers. Conclusion from EDS:
The elemental analysis quantitatively confirmed the morphological observations: 5% Ni content produces optimal conditions for maximum Cu_2O deposition with superior uniformity compared to lower or higher Ni concentrations.

3.3 Crystallographic Analysis (XRD)

X-ray diffraction patterns provided definitive phase identification and crystallinity assessment.
Cu_2O Phase Confirmation:
All Cu_2O-coated samples exhibited characteristic diffraction peaks matching the standard cuprite (Cu_2O) crystal structure:
Major Cu_2O peaks:

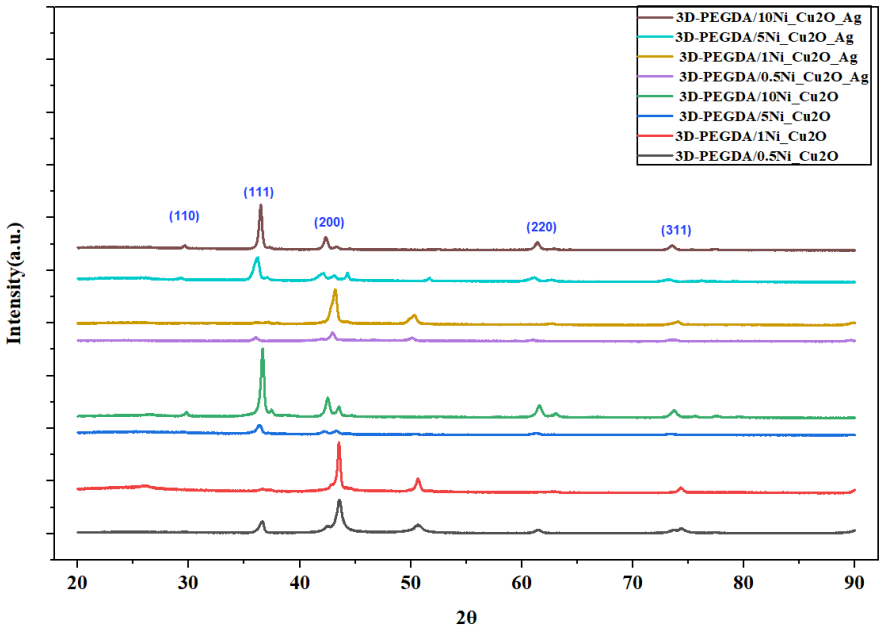

- ∼29.6° (2θ) → (110) plane
- ∼36.4° (2θ) → (111) plane
- ∼42.3° (2θ) → (200) plane
- ∼61.4° (2θ) → (220) plane
- ∼73.5° (2θ) → (311) plane

The presence of these peaks confirmed successful Cu_2O formation rather than metallic copper (which would show peaks at different positions) or other copper compounds.

Influence of Nickel Content on Crystallinity:
A clear trend emerged as Ni content varied:

- 0.5% Ni: Broad, low-intensity Cu_2O peaks indicating small crystallite size and/or lower crystallinity.
- 1% Ni: Slightly improved peak intensity and definition.
- 5% Ni: Sharpest, most intense Cu_2O peaks indicating:
  - Larger crystallite size (Scherrer equation)
  - Higher degree of crystallinity
  - Improved long-range structural order
  - Greater quantity of Cu_2O phase
- 10% Ni: Peak intensity increases indicating greater crystallanity.

Silver Phase Detection:
In Ag-decorated samples, additional peaks appeared at:

- 38.1° (2θ) → Ag (111)
- ∼44.3° (2θ) → Ag (200)
- ∼64.4° (2θ) → Ag (220)

These peaks confirmed successful Ag deposition. However, their relatively low intensity compared to Cu_2O peaks indicated:

- Small amount of Ag compared to Cu_2O.
- Highly dispersed or very fine Ag nanostructures.
- Possible low crystallinity of Ag nanowires.

Interpretation: The XRD results quantitatively demonstrated that higher Ni provides ideal conditions for Cu_2O crystal growth.
The enhanced crystallinity at this composition suggests that Ni facilitates:

- More efficient nucleation creating numerous growth centers.
- Stable growth conditions allowing crystals to develop without premature termination.
- Proper local chemistry maintaining Cu_2O phase stability.

3.4 Raman Spectroscopy Analysis

Raman spectroscopy provided complementary structural confirmation and quantitative comparison of Cu_2O content.

Cu_2O Characteristic Peak:

All Cu_2O-containing samples exhibited a prominent Raman peak at approximately 147-150 cm^1. This peak arises from the symmetric stretching vibrational mode of oxygen atoms within the cuprite (Cu_2O) crystal lattice. The Cu-O-Cu bond angle and symmetry in the cubic structure produce this characteristic Raman-active phonon mode.

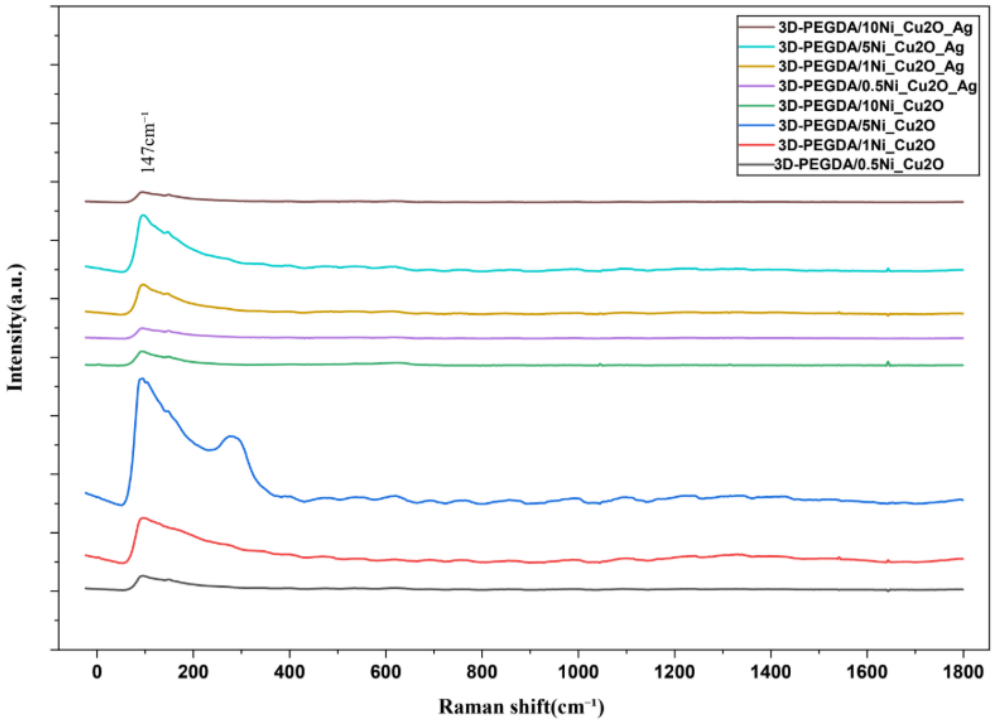

Significance: This peak is diagnostic for Cu_2O and distinguishes it from:

- CuO: Would exhibit Raman peaks at ∼290 cm^{-1}, ∼340 cm^{-1}, and ∼630 cm^{-1}.
- Metallic Cu: Raman-inactive.
- $Cu(OH)_2$: Shows different characteristic peak positions.

Intensity Trend Analysis: The Raman peak intensity at 147 cm^1 served as a quantitative measure of Cu_2O content and crystalline quality. Relative Intensity Progression:

- 0.5% Ni: Weak intensity (baseline).
- 1% Ni: Moderate intensity (2–3× increase over 0.5%).

- 5% Ni: Maximum intensity (5–6× increase over 0.5%; strongest signal).
- 10% Ni: Decreased intensity (3–4× baseline; clear drop from 5%).

Key Observation:
The Raman intensity follows the same trend observed in SEM, EDS, and XRD: progressive increase from 0.5% → 1% → peak at 5% Ni → decline at 10% Ni. This multi-technique concordance provides robust evidence that 5% Ni represents the optimal composition for CuO formation.
Physical Interpretation:
Higher Raman intensity indicates:

- A greater quantity of Cu_2O phase present.
- Better crystalline order, resulting in more well-defined lattice vibrations.
- Larger crystallite domains.
- Higher purity of the Cu_2O phase without competing phases.

The peak sharpness (full width at half maximum - FWHM) also narrowed at 5% Ni, suggesting improved long-range structural order and reduced lattice defects or strain.

3.5 Photocatalytic Performance

The ultimate test of the synthesized materials was their ability to degrade methylene blue under visible light irradiation.
Experimental Setup:

- Methylene blue concentration: Typically 10–20 ppm aqueous solution.
- Light source: Visible light (solar simulator or LED lamp with $\lambda > 400$ nm).
- Catalyst loading: Standardized mass or surface area of the microlattice sample.
- Reaction vessel: Quartz or glass beaker allowing proper light penetration.
- Monitoring: UV–Vis spectroscopy at regular time intervals (0, 30, 60, 90, 120, 150, 180 minutes).

Visual Observations:
Time-lapse photography documented the progressive decolorization of methylene blue solution:
3D-PEGDA/%5Ni_Cu_2O:

- 0 min: Intense blue color (high MB concentration).
- 30 min: Slightly lighter blue.
- 60 min: Noticeably faded blue.
- 90 min: Pale blue.
- 120 min: Very light blue.
- 150 min: Nearly colorless.
- 180 min: Almost complete decolorization.

3D-PEGDA/%5Ni_Cu_2O_Ag:

- 0 min: Intense blue color.
- 30 min: Significantly lighter (faster degradation than non-Ag sample).
- 60 min: Pale blue (more advanced than Cu_2O-only at the same time).
- 90 min: Very light blue.
- 120 min: Nearly colorless.
- 150 min: Complete decolorization.
- 180 min: Colorless (complete degradation).

Quantitative Degradation Analysis:
UV-Vis absorption measurements at = 664 nm (MB characteristic peak) were used to calculate degradation efficiency:

$$\text{Degradation (\%)} = \frac{A_0 - A_t}{A_0} \times 100$$

where A = initial absorbance, A = absorbance at time t

Results Summary:
Sample60 min (%)120 min (%)180 min (%)0.5% Ni Cu_2O 20-25 35-40 50-551% Ni CuO 30-35 50-55 65-705% Ni CuO 45-50 75-80 90-9510% Ni CuO 25-30 45-50 60-655% Ni CuO+Ag 60-65 88-92 98-99

Key Findings:
5% Ni optimal: The 5% Ni sample without Ag achieved 90-95% degradation in 180 minutes, significantly outperforming all other Ni concentrations.
Silver enhancement: Adding Ag nanowires to the 5% Ni sample boosted degradation to 98-99% in the same timeframe, with notably faster kinetics in the early stages.
Ni content correlation: Photocatalytic performance directly correlated with Cu_2O loading and crystallinity as determined by characterization techniques.
Reaction kinetics: The degradation followed pseudo-first-order kinetics, typical for photocatalytic reactions:

$$\ln\left(\frac{C}{C_0}\right) = -kt$$

Rate constant k highest for 5% Ni + Ag sample

Comparison with Control Experiments:

- Dark control: Negligible MB degradation ($< 5\%$ in 180 min), confirming the need for photocatalytic activation.
- Light only (no catalyst): Minimal degradation ($\sim$10–15%) due to direct photolysis.
- PyC substrate only: Low activity ($\sim$20–25%) because of limited ROS generation.
- Commercial TiO_2 reference: Performance comparable to or better than P25 TiO_2 under visible light.

Mechanism Confirmation: The visible-light activity confirms Cu_2O's suitable band gap (2.0-2.2 eV) for solar spectrum absorption. The Ag enhancement suggests successful plasmonic coupling and charge separation improvement. The correlation between Cu_2O loading and activity validates the material design strategy.

3.6 Effect of Nickel Content on Cu_2O Deposition

The systematic variation in Cu_2O formation with Ni content requires detailed mechanistic explanation. The experimental observations reveal a non-monotonic relationship: performance increases from 0.5% → 1% → 5% Ni (optimal) → decreases at 10% Ni.

3.6.1 Why Low Ni Content (0.5% and 1%) Produces Less Cu_2O

At very low nickel concentrations, the pyrolytic carbon substrate remains predominantly carbon with only sparse Ni particles distributed throughout. This composition imposes several limitations:

- **Insufficient Catalytic Activity:** Nickel particles act as catalytic sites for electrochemical reactions. At low Ni content:
  - Few active sites are available for Cu^{2+} ion reduction.
  - Large carbon-only regions exhibit slower electron transfer kinetics.
  - The overall surface shows heterogeneous reactivity with significant "cold spots" of low activity.
- **Poor Electrical Conductivity:** While pyrolytic carbon is moderately conductive, nickel metal is significantly more conductive:
  - Conductivity of PyC: $\sim 10^2$–10^3 S/m.
  - Conductivity of Ni: $\sim 1.4 \times 10^7$ S/m (over 10,000× higher).

  At 0.5–1% Ni, the improvement in substrate conductivity is minimal, causing:
  - Higher overpotential required for Cu^{2+} reduction.
  - Slower electron transfer from electrode to Cu^{2+} ions.
  - Kinetically limited deposition rate.
- **Limited Nucleation Sites:** Ni provides high-energy heterogeneous nucleation sites because of:
  - Higher surface energy than carbon ($\gamma_{Ni} > \gamma_C$).
  - Favorable lattice matching or electronic interactions.
  - Local electric-field enhancement at Ni–carbon interfaces.

  With sparse Ni distribution:
  - Insufficient nucleation centers are available.

- Cu_2O crystals nucleate slowly and sparsely.
- Growth occurs on only a few points, forming large crystals in isolated regions rather than a uniform fine-grained coating.

- **Slow Cu_2O Crystal Growth:** Even after nucleation, Cu_2O crystal growth requires:
  - Continuous electron supply for $Cu^{2+} \rightarrow Cu^{+}$ reduction.
  - Stable local chemistry (pH, ion concentration).
  - Efficient charge transfer through the substrate.

Low Ni content creates bottlenecks in all these aspects, resulting in:

Thin, incomplete Cu_2O films Patchy coverage with bare carbon exposed Small total Cu_2O mass Weak Raman and XRD signals

Summary: At 0.5-1% Ni, the substrate lacks sufficient catalytic sites, conductivity, and nucleation centers to support robust Cu_2O formation.

3.6.2 Why 5% Ni is Optimal for Maximum CuO Deposition

At 5% Ni, a critical balance is achieved that maximizes CuO formation through multiple synergistic effects:

- **Enhanced Electrical Conductivity:** The increased Ni content significantly improves substrate conductivity without overwhelming the carbon matrix:
  - Ni particles create conductive pathways throughout the structure.
  - Electrons flow readily from the external circuit to the electrolyte interface.
  - Lower overpotential is required for Cu^{2+} reduction.
  - Uniform current distribution occurs across the microlattice surface.

  Result: Fast, efficient electron transfer enabling rapid $Cu^{2+} \rightarrow Cu^{+}$ reduction at lower applied voltage.

- **Abundant High-Energy Nucleation Sites:** With 5% Ni, the particle distribution reaches optimal density:
  - Numerous Ni sites are distributed across the carbon surface.
  - High surface energy at Ni locations favors ion adsorption.
  - Favorable energetics exist for Cu_2O embryo formation.
  - Reduced critical nucleus size makes nucleation easier.

Physical explanation: The interfacial energy between nucleus and substrate ($\gamma_{\text{nucleus-substrate}}$) is lower at Ni sites than on carbon. This reduces the Gibbs free energy barrier (ΔG^*) for nucleation:

$$\Delta G^* \propto \frac{\gamma^3}{(\Delta\mu)^2}$$

where $\Delta\mu$ is the chemical potential driving force. Lower $\gamma \rightarrow$ lower $\Delta G^* \rightarrow$ faster nucleation rate.

Result: High nucleation density creates many small crystals rather than few large ones, leading to:

- Uniform, fine-grained Cu_2O coating.
- Complete surface coverage.
- High total surface area of Cu_2O (more active photocatalytic sites).

- **Stable Local pH During Deposition:** The electrodeposition process involves OH^- generation as a byproduct:

$$2H_2O + 2e^- \rightarrow H_2 + 2OH^-$$

and Cu_2O formation proceeds via:

$$Cu^{2+} + 2OH^- \rightarrow Cu(OH)_2 \rightarrow Cu_2O + H_2O$$

At 5% Ni, the balance of reaction rates maintains stable local pH:

- Enough OH^- is generated to promote Cu_2O formation under alkaline conditions.
- OH^- does not accumulate excessively to cause uncontrolled precipitation.
- Lactic acid in the electrolyte helps buffer local pH.
- Uniform pH across the surface ensures uniform deposition.

Result: Consistent Cu_2O formation conditions across the entire substrate surface without localized precipitation or dissolution.

- **Optimal Reduction Potential:** The applied voltage (5 V) together with 5% Ni conductivity creates the ideal electrochemical potential at the surface:

- Sufficient driving force for $Cu^{2+} \rightarrow Cu^+$ reduction.
- Prevents overly negative potentials that would favor $Cu^{2+} \rightarrow Cu^0$ (metallic copper).
- Maintains stability of the Cu^+ oxidation state.
- Supports selective Cu_2O formation over CuO or Cu metal.

- **Favorable Charge Transfer Kinetics:** The pulse deposition parameters (50 Hz, 40% duty cycle) work optimally with 5% Ni:

- **ON period:** Rapid reduction occurs at Ni-enhanced conductive sites.
- **OFF period:** Allows Cu^{2+} replenishment via diffusion from the bulk electrolyte.
- Prevents depletion-layer buildup near electrode surface.
- Maintains a stable concentration gradient for continuous ion supply.

- **Synergistic Cu_2O Growth:** Once nucleated, Cu_2O crystals grow efficiently at 5% Ni because:
  - Continuous electron supply is provided through conductive Ni pathways.
  - Growth environment remains stable (pH, potential, ion availability).
  - Growth rate is uniform across all nucleation sites.
  - Adjacent crystals coalesce to form a continuous film.

  Result: The combination of these factors produces:
  - Maximum Cu_2O loading (highest deposited mass).
  - Best crystallinity (sharpest XRD peaks).
  - Most uniform coverage (confirmed by SEM imaging).
  - Strongest Raman signal at $\sim$147 cm^{-1}.
  - Superior photocatalytic performance.

  Summary: 5% Ni represents the "sweet spot" where catalytic activity, conductivity, nucleation density, and growth conditions are all optimized simultaneously.

3.6.3 Why Excessive Ni Content (10%) Reduces CuO Formation

At 10% Ni, the benefits observed at 5% are lost due to several detrimental effects arising from over-abundance of Ni:

- **Overly Conductive Surface:** Excessive Ni makes the substrate too conductive, altering electrochemical behavior:
  - Fast electron flow pushes electrode potential very negative (cathodic).
  - This shifts the reduction equilibrium:
    - Moderate potential: $Cu^{2+} + e^- \rightarrow Cu^+$ (desired, forms Cu_2O)
    - Very negative potential: $Cu^{2+} + 2e^- \rightarrow Cu^0$ (undesired, forms metallic Cu)
  - Metallic Cu forms non-uniformly at high Ni:
    - Preferential deposition on Ni sites.
    - 3D dendritic or powdery growth instead of a smooth film.

        - Poor adhesion causes detachment.
    - Overall Cu deposition decreases despite favorable potential.

- **Enhanced Hydrogen Evolution Reaction (HER):** Nickel strongly catalyzes hydrogen evolution:

$$2H^+ + 2e^- \rightarrow H_2 \qquad \text{(acidic)}$$

$$2H_2O + 2e^- \rightarrow H_2 + 2OH^- \qquad \text{(alkaline)}$$

  At 10% Ni, HER becomes a dominant competing reaction:

    - **Direct competition:**
        - Electrons are consumed by HER instead of Cu^{2+} reduction.
        - Current efficiency for Cu deposition decreases.
        - Less Cu^{2+} gets reduced overall.
    - **Physical blocking by bubbles:**
        - H_2 bubbles adhere to the surface.
        - Bubbles block Cu^{2+} access to active sites.
        - Gas pockets disrupt uniform deposition.
    - **Mass transport limitations:**
        - Bubble formation disturbs the diffusion boundary layer.
        - Cu^{2+} concentration fluctuates at the surface.
        - Deposition becomes highly non-uniform.

  Result: Large fraction of applied current is wasted on H_2 evolution instead of Cu_2O formation.

- **Unstable Local pH:** Excessive HER dramatically increases local OH^- concentration:

    - Rapid OH^- generation pushes pH to 12–14 near the surface.
    - Local pH fluctuates depending on Ni density.

  Consequences:

    - **Uncontrolled precipitation:**

$$Cu^{2+} + 2OH^- \rightarrow Cu(OH)_2 \downarrow$$

    - Precipitate forms in solution instead of depositing.
    - Loose precipitate may detach → loss of Cu.
    - **Phase instability:**
        - Very high pH may convert Cu_2O to CuO.
        - Mixed phases with poor crystallinity form.
    - **Non-uniform chemistry:**

- Some regions form Cu_2O, others CuO or Cu metal.
- Surface becomes compositionally heterogeneous.

– **Cu Redissolution:** At very alkaline pH and strongly reducing conditions:

* Cu^+ becomes unstable.
* Deposited Cu may dissolve back into solution as soluble complexes.
* Dynamic deposition/dissolution cycle prevents film buildup.

Result: Net Cu_2O formation decreases despite initial deposition.

– **Altered Nucleation Behavior:** At 10% Ni, nucleation becomes suboptimal:

* Too many nucleation sites compete for limited Cu^{2+}.
* Local depletion of Cu^{2+} around high-density Ni regions.
* Nuclei remain small and cannot grow properly.
* Poor coalescence prevents formation of continuous film.

– **Structural Defects:** Rapid and unstable deposition creates:

* High density of crystal defects (dislocations, grain boundaries).
* Lattice strain (broadened XRD peaks).
* Reduced crystallinity (weak Raman signal).
* Poor-quality Cu_2O even where deposition occurs.

Summary of 10% Ni Effects:

– Combined impact of:

* Over-reduction favoring Cu^0 formation (but poorly deposited).
* Competing hydrogen evolution reaction (HER) consuming electrons.
* Surface blocking by H_2 bubbles.
* Unstable pH disrupting deposition chemistry.
* Possible redissolution of deposited Cu.

– Results in:

* Lower total Cu_2O deposition.
* Poor crystallinity (broadened XRD peaks, weaker Raman signal).
* Patchy, non-uniform surface coverage (SEM evidence).
* Reduced photocatalytic activity.

3.6.4 Overall Trend Summary

The experimental data across all characterization techniques reveals a consistent pattern:

0.5% Ni: Low Cu_2O (insufficient catalysis/conductivity)

↓

1% Ni: Moderate Cu_2O (improving but still limited)

↓

5% Ni: Cu_2O (optimal balance)

↓

10% Ni: Reduced Cu_2O (over-reduction, competing reactions)

This non-monotonic relationship demonstrates a classic optimization problem:
Too little Ni fails to provide adequate enhancement; too much Ni introduces detrimental side effects. The 5% composition achieves the ideal balance.
Photocatalytic Performance Correlation:
The MB degradation efficiency directly tracks Cu_2O loading and quality:

More Cu_2O → more photocatalytic active sites Better crystallinity → better charge separation Uniform coverage → consistent ROS generation Ag enhancement → further improved efficiency

Therefore, the 5% Ni sample with Ag decoration achieves maximum performance (98-99% degradation in 180 min).

4

Conclusion

4.1 Key Findings

This project successfully demonstrated the fabrication and optimization of CuO-decorated pyrolytic carbon microlattice photocatalysts for visible-light-driven methylene blue degradation. The key findings are:

- **Optimal Nickel Content:** Nickel content in the carbon substrate critically influences Cu_2O deposition. Among all tested compositions (0.5%, 1%, 5%, 10%), 5% Ni yielded maximum Cu_2O loading with superior crystallinity and uniform surface coverage. This optimal composition represents a balance between beneficial effects (enhanced conductivity, catalytic sites, nucleation centers) and detrimental effects (over-reduction, competing HER, pH instability).
- **Multi-Technique Concordance:** All characterization methods—SEM, EDS, XRD, and Raman spectroscopy—independently confirmed the same trend: Cu_2O formation increases progressively from 0.5% → 1% → peaks at 5% Ni → decreases at 10% Ni. This multi-modal validation provides robust evidence for the optimal composition.
- **Mechanistic Understanding:** The project elucidated the underlying mechanisms governing Ni–Cu_2O relationships:
  - **Low Ni (0.5–1%):** Limited by insufficient electron transfer, sparse nucleation sites, and slow crystal growth.
  - **Optimal Ni (5%):** Benefits from enhanced conductivity, abundant nucleation sites, stable pH, and favorable electrochemical potential.
  - **High Ni (10%):** Suffers from over-reduction to Cu^0, competing hydrogen evolution, surface blocking by H_2 bubbles, and unstable local chemistry.
- **Silver Enhancement:** Drop-casting silver nanowires onto Cu_2O-coated samples significantly improved photocatalytic performance. The 5% Ni sample with Ag decoration achieved ∼98–99% methylene blue degradation in 180 minutes, outperforming

the non-decorated sample (∼90–95%). The Ag enhancement likely operates through plasmonic effects, electron trapping, and co-catalytic ROS generation.

- **Photocatalytic Efficiency:** The optimized (Ag/Cu_2O)@PyC photocatalyst demonstrated excellent visible-light activity for MB degradation, addressing a critical water contamination problem. The 3D microlattice architecture enabled:
  - Deep light penetration,
  - High catalyst loading,
  - Efficient mass transport,

  giving advantages over conventional planar or powder catalysts.
- **Structure–Property Relationships:** The project established clear correlations between:
  - Ni content → Cu_2O loading → crystallinity → photocatalytic performance.
  - Material structure (microlattice) → light utilization → ROS generation → pollutant degradation.

  These relationships provide design principles for future photocatalyst development.

4.2 Future Scope

While this project achieved its objectives, several avenues for future investigation remain:

- **Mechanistic Studies:**
  - Detailed electrochemical impedance spectroscopy (EIS) to quantify charge transfer resistance as a function of Ni content.
  - In-situ pH mapping during electrodeposition to visualize local chemistry changes.
  - Computational modeling (DFT calculations) of Cu_2O nucleation energetics on Ni vs. carbon sites.
  - Time-resolved spectroscopy to track charge carrier dynamics and recombination processes.
- **Optimization Refinement:**
  - Fine-tuning Ni content in narrower ranges (e.g., 4%, 4.5%, 5%, 5.5%, 6%) to precisely identify the optimum.
  - Varying electrodeposition parameters (frequency, voltage, duty cycle, time) to maximize Cu_2O quality.
  - Testing different Ag loading amounts and morphologies (nanoparticles vs. nanowires vs. nanoflakes).
  - Exploring ternary composites (e.g., Ag–Cu_2O–graphene or additional metal co-catalysts).

- **Extended Pollutant Testing:**
  - Evaluating performance against other organic dyes (Rhodamine B, Methyl Orange, Congo Red).
  - Testing pharmaceutical contaminants (antibiotics, hormones).
  - Assessing effectiveness for pesticide degradation.
  - Investigating mixed pollutant scenarios representative of real industrial wastewater.
- **Stability and Reusability:**
  - Long-term cycling experiments (20–50 cycles) to assess catalyst durability.
  - Investigating potential Cu_2O photocorrosion and developing strategies to mitigate it.
  - Testing catalyst regeneration protocols for practical applications.
  - Evaluating performance degradation mechanisms and surface passivation effects.
- **Scale-Up and Practical Implementation:**
  - Designing continuous-flow photocatalytic reactors incorporating microlattice catalysts.
  - Economic analysis comparing costs to conventional water treatment methods.
  - Pilot-scale testing with actual industrial wastewater.
  - Integration with solar concentrators for enhanced outdoor performance.
- **Alternative Material Systems:**
  - Substituting other transition metals (Co, Fe, Mn) for Ni to compare catalytic effects.
  - Testing alternative semiconductor oxides (ZnO, WO_3, $BiVO_4$) on the same substrate.
  - Investigating sulfide or nitride semiconductors for enhanced visible-light absorption.
  - Exploring perovskite photocatalysts on 3D carbon supports.
- **Advanced Characterization:**
  - Transmission electron microscopy (TEM) for atomic-scale interface characterization.
  - X-ray photoelectron spectroscopy (XPS) to analyze surface chemistry and oxidation states.
  - Photoluminescence (PL) spectroscopy to study charge recombination kinetics.
  - Electrochemical Mott–Schottky analysis to determine band positions and carrier densities.
- **Broader Applications:**

* Adapting the catalyst for CO_2 photoreduction to produce solar fuels.
* Investigating photoelectrochemical water splitting for hydrogen generation.
* Exploring antibacterial applications using ROS generation.
* Developing sensors based on photocatalytic responses to specific analytes.

4.3 Concluding Remarks

This B.Tech project demonstrated successful integration of advanced manufacturing (DLP 3D printing), materials processing (pyrolysis, electrodeposition), and catalysis to address a significant environmental challenge. The systematic investigation of Ni content effects provided fundamental insights into catalyst optimization while achieving practical water purification capabilities. The optimized (Ag/Cu_2O)@PyC photocatalyst represents a promising technology for sustainable water treatment, with potential for further development toward commercial applications. The comprehensive characterization and mechanistic understanding developed in this work establish a foundation for future research in structured photocatalysts and provide valuable design principles for materials engineers working on environmental remediation technologies.

Appendix A

Appendix

A.1 Photocatalytic Reaction Mechanism Details

Complete Reaction Pathway:

1. **Photon Absorption and Charge Generation**

$$\mathrm{Cu_2O} + \mathrm{h}\nu \text{ (visible)} \rightarrow \mathrm{e^-_{CB}} + \mathrm{h^+_{VB}}$$

When photons with energy $\geq$ the Cu_2O bandgap ($\sim$2.0–2.2 eV) are absorbed, electrons are excited from the valence band to the conduction band, generating electron–hole pairs.

2. **Charge Separation and Transfer**

$$e^-_{CB}(\mathrm{Cu_2O}) \rightarrow e^-(\mathrm{Ag/PyC})$$

$$\mathrm{Ag} + \mathrm{h}\nu \rightarrow \mathrm{Ag^*} \rightarrow \text{hot electrons}$$

Electrons transfer to Ag nanowires or the PyC substrate, suppressing recombination. Ag also produces hot electrons via surface plasmon resonance.

3. **Oxygen Reduction to Superoxide**

$$\mathrm{O_2} + \mathrm{e^-} \rightarrow \cdot\mathrm{O_2^-}$$

Conduction-band electrons reduce dissolved oxygen to superoxide radicals.

4. **Formation of Hydroperoxyl and Hydrogen Peroxide**

$$\cdot\mathrm{O_2^-} + \mathrm{H^+} \rightarrow \mathrm{HO_2^\cdot}$$

$$2 \cdot O_2^- + 2H^+ \rightarrow H_2O_2 + O_2$$

$$HO_2^{\cdot} + e^- + H^+ \rightarrow H_2O_2$$

Superoxide undergoes protonation and disproportionation to form hydroperoxyl radicals and hydrogen peroxide.

5. **Hydroxyl Radical Generation**

$$H_2O_2 + e^- \rightarrow \cdot OH + OH^-$$

$$H_2O_2 + h\nu \rightarrow 2 \cdot OH$$

$$H_2O_2 \xrightarrow[\text{Ag surface}]{} 2 \cdot OH$$

Hydrogen peroxide decomposes to form hydroxyl radicals, the strongest oxidizing species.

6. **Direct Hole Oxidation (Alternative Pathway)**

$$h^+ + OH^- \rightarrow \cdot OH$$

$$h^+ + H_2O \rightarrow \cdot OH + H^+$$

Holes can directly oxidize water or hydroxide ions to generate hydroxyl radicals.

7. **Pollutant Oxidation and Mineralization**

$$MB + (\cdot OH,\ h^+,\ \cdot O_2^-) \rightarrow \text{ intermediates} \rightarrow CO_2 + H_2O + NH_4^+ + SO_4^{2-}$$

Reactive oxygen species degrade methylene blue by attacking C–N, C–S, and C–C bonds, leading to complete mineralization.

A.2 Experimental Parameters Summary

3D Printing Parameters:

- **Technology:** Digital Light Processing (DLP)
- **Resin:** PEGDA (polyethylene glycol diacrylate)
- **Nickel Content:** 0.5%, 1%, 5%, and 10% by weight
- **Layer Thickness:** 50–100 μm
- **Exposure Time:** 5–15 seconds per layer

Pyrolysis Parameters:

- **Temperature:** 900°C
- **Atmosphere:** Argon or nitrogen
- **Heating Rate:** 5–10°C/min
- **Holding Time:** 1–2 hours
- **Cooling:** Natural cooling under inert gas

Electrodeposition Parameter

- **Electrolyte Composition:**
  - $CuSO_4 \cdot 5H_2O$ (0.75%)
  - NaOH (1.6%)
  - Lactic acid (3.9%)
- **Voltage:** 5 V
- **Frequency:** 50 Hz
- **Duty Cycle:** 40%
- **Deposition Time:** 10–30 minutes
- **Temperature:** Room temperature (25°C)

Photocatalytic Testing Parameters:

- **MB Concentration:** 10–20 ppm
- **Catalyst Loading:** Standardized surface area
- **Light Source:** Visible light ($\lambda > 400$ nm, intensity $\sim$100 mW/cm^2)
- **Reaction Time:** 0–180 minutes
- **Temperature:** Room temperature
- **Sampling Intervals:** Every 30 minutes

Appendix B

References

- Evaluation of the Structural Deviation of Cu/Cu_2O Nanocomposite Using the X-ray Diffraction Analysis Methods
- Visible Light Driven Heterojunction Photocatalyst of CuO–Cu_2O Thin Films for Photocatalytic Degradation of Organic Pollutants
- Phases Evolution and Photocatalytic Activity of Cu_2O Films Electrodeposited from a Non-pH-Adjusted Solution
- ZnO/CuO Nanostructures Anchored over Ni/Cu Tubular Films via Pulse Electrodeposition for Photocatalytic and Antibacterial Applications
- Application of a Fully 3D Printed Carbon Electrode for the Double Potential Step Chronoamperometric Determination of 2,4-Dinitrophenol in Environmental Water Samples
- Integrated Electrochemical and Photocatalytic Degradation Using ZnO Caterpillars Photocatalyst: Two-Step Approach for Textile Industry Based Wastewater Recovery
- ZnO Nanowire-Decorated 3D Printed Pyrolytic Carbon for Solar Light–Driven Photocatalytic Degradation of Wastewater Contaminants